

# Implications of NANOGrav results and UV freeze-in in a fast-expanding Universe

Basabendu Barman,<sup>1,\*</sup> Amit Dutta Banik,<sup>2,†</sup> and Avik Paul<sup>3,‡</sup>

<sup>1</sup>*Department of Physics, IIT Guwahati, Guwahati-781039, India*

<sup>2</sup>*Key Laboratory of Quark and Lepton Physics (MoE) and Institute of Particle Physics, Central China Normal University, Wuhan 430079, China*

<sup>3</sup>*Astroparticle Physics and Cosmology Division, Saha Institute of Nuclear Physics, HBNI, 1/AF Bidhannagar, Kolkata 700064, India*

Recent pulsar timing data reported by the NANOGrav collaboration indicates the existence of a stochastic gravitational wave (GW) background at a frequency  $f \sim 10^{-8}$  Hz. We show that a dark sector consisting of a Standard Model (SM) gauge singlet fermion  $\chi$  and a singlet scalar  $\phi$ , both charged under a  $Z_4$  symmetry, is capable of generating such a low frequency GW via strong first order phase transition (SFOPT) through the modification of the standard cosmological history, where we assume faster-than-usual expansion at pre-BBN times driven by a new cosmological species  $\varphi$  whose energy density red-shifts with the scale factor as  $\rho_\varphi \propto a^{-(4+n)}$ . Depending on the choice of the fast expansion parameters, reheat temperature and effective scale of the theory, it is also possible to address correct dark matter (DM) relic abundance via freeze-in. We show that a successful first order phase transition explaining NANOGrav results together with PLANCK observed DM abundance put bound on the fast expansion parameters requiring  $n \lesssim 4$  to explain both.

## I. INTRODUCTION

Recently, the North American Nanohertz Observatory for Gravitational Waves (NANOGrav) has reported a possible detection of a Stochastic gravitational wave background (SGWB) with their 12.5 year data set of the pulsar timing array [1] that may be interpreted as a gravitational wave (GW) signal with amplitude of  $\sim \mathcal{O}(10^{-15})$  at a reference frequency of  $f_{\text{yr}} = 1\text{yr}^{-1}$ . The NANOGrav collaboration has found no evidence of monopolar or dipolar correlations which may arise from reference clock or solar-system ephemeris systematics, they also claim that there is no statistically significant evidence that this process has quadrupolar spatial correlations which can be a *smoking gun* for GW background. However, several attempts were proposed, so as to interpret the NANOGrav observations which include supermassive black hole merger events [1, 2], cosmic strings [3–5], magneto-hydrodynamic (MHD) turbulence at a first-order cosmological QCD phase transition [6] or phase transition from a hidden sector [7]. As shown in [8] the NANOGrav data can be well explained as a GW signal from first order phase transition (FOPT) around the warm dark matter (DM) physics scale that lies in the keV-MeV range, well below the electroweak scale. In [9] it was shown that NANOGrav observation can be explained by the first order GWs in the nonstandard thermal history with an early matter dominated (EMD) era.

The expansion rate of the universe is parametrized by the Hubble parameter which is directly related to the total energy density of the universe through standard Friedman equations [10]. In the standard case, it is assumed that the universe was radiation dominated before

Big Bang Nucleosynthesis (BBN). However, there are no fundamental reasons to assume that the universe was radiation-dominated prior to BBN at  $t \sim 1$  sec. The absence of any direct evidence that the universe was indeed only radiation dominated in the pre-BBN era compels us to explore a modified cosmological scenario where the expansion rate of the universe naturally alters from what it is in case of the standard scenario. The influence of the presence of another species that drives the expansion of the universe faster than the standard cosmological history on DM yield has been studied in detail both in the context of Weakly Interacting Massive Particle (WIMP) [11] and Feebly Interacting Massive Particle (FIMP) [12]. In case of DM *freeze-in* it has been shown that in a fast expanding universe the DM production via decay and/or annihilation of the bath particles is dramatically suppressed that demands a larger coupling between the dark and the visible sector to satisfy the observed relic abundance. This sheds some optimistic prospects on detecting DM produced via freeze-in which otherwise is extremely difficult to detect.

Motivated from all these in this work we propose a simple framework where we assume the presence of another species  $\varphi$  whose energy density red-shifts with the scale factor as  $\rho_\varphi \propto a^{-(4+n)}$ . For  $n > 0$  the  $\varphi$  energy density dominates over radiation at early enough times. However, the equality between  $\rho_\varphi$  and  $\rho_{\text{rad}}$  happens at a temperature  $T_R \gtrsim T_{\text{BBN}}$ . This, as one can understand, alters the Hubble parameter leading to a faster-than-usual-expansion of the universe in the pre-BBN era. In such a modified cosmological background we consider a simple dark sector made up of a Standard Model (SM) gauge singlet fermion  $\chi$  and a singlet scalar  $\phi$  both charged under a  $Z_4$  symmetry. We assume  $\chi$  is lighter than  $\phi$  and hence it serves as a potential DM candidate. The lack of any renormalizable interaction between the dark sector and the SM motivates the DM production via Ultra-violate (UV) freeze-in [13–15].

\* E-mail: [bb1988@iitg.ac.in](mailto:bb1988@iitg.ac.in)

† E-mail: [amitdbanik@mail.ccnu.edu.cn](mailto:amitdbanik@mail.ccnu.edu.cn)

‡ E-mail: [avik.paul@saha.ac.in](mailto:avik.paul@saha.ac.in)

The requirement of satisfying PLANCK observed [16, 17] relic abundance constraints the reheat temperature, effective scale of the theory and also the fast expansion parameters  $n$  and  $T_R$ . The singlet scalar, on the other hand, triggers a strong first order electroweak phase transition (SFOPT) that generates detectable GW signal. We show, in a fast expanding universe such GW signals<sup>1</sup> generated from electroweak phase transition can explain the NANOGrav 12.5 yrs data within  $2\sigma$  confidence. The requirement of producing right DM abundance together with GW signal satisfying NANOGrav results put bound on the fast expansion parameters, typically requiring  $n \lesssim 4$  and  $T_R \sim \mathcal{O}(100)$  MeV.

The paper is organized as follows: in Sec. II we describe the modification in the Hubble parameter due to fast expansion; the effect of modified Hubble parameter on DM yield in the context of a toy model is detailed in Sec. III; in Sec. IV we discuss the generation of detectable GW signal from strong first order phase transition that is capable of explaining the NANOGrav 12.5 yrs data; we then briefly touch upon a possible UV completion for this toy model in Sec. V and finally we conclude in Sec. VI.

## II. A FAST EXPANDING UNIVERSE

As mentioned in Sec. I, we assume the universe before BBN has two different species: radiation and some other species  $\varphi$  with energy densities  $\rho_{\text{rad}}$  and  $\rho_\varphi$  respectively. In presence of a new species ( $\varphi$ ) along with the radiation field, the total energy budget of the universe is  $\rho = \rho_{\text{rad}} + \rho_\varphi$ . One can always express the energy density of the radiation component as function of temperature  $T$  [10]

$$\rho_{\text{rad}}(T) = \frac{\pi^2}{30} g_*(T) T^4 \quad (1)$$

with  $g_*(T)$  being the effective number of relativistic degrees of freedom at temperature  $T$ . In the absence of entropy production per comoving volume *i.e.*  $sa^3 = \text{const.}$ , radiation energy density redshifts as  $\rho_{\text{rad}}(t) \propto a(t)^{-4}$ . In case of a rapid expansion of the universe the energy density of  $\varphi$  field is expected to be redshifted faster than the radiation. Accordingly, one can assume  $\rho_\varphi \propto a(t)^{-(4+n)}$ . Thus  $n > 0$  implies that  $\varphi$  energy density dominates over radiation at early enough times.

Now, the entropy density (per comoving volume) of the universe is expressed as

$$s(T) = \frac{2\pi^2}{45} g_{*s}(T) T^3$$

where  $g_{*s}(T)$  is the effective relativistic degrees of freedom. A general form of  $\rho_\varphi$  can then be constructed using

the entropy conservation  $g_*(T)^{1/3} aT = \text{constant}$  in a comoving frame as:

$$\rho_\varphi(T) = \rho_\varphi(T_R) \left( \frac{g_{*s}(T)}{g_{*s}(T_R)} \right)^{(4+n)/3} \left( \frac{T}{T_R} \right)^{(4+n)}. \quad (2)$$

The temperature  $T_R$  is an unknown variable and can be considered as the point of equality where the two fluids have equal energy densities:  $\rho_\varphi(T_R) = \rho_{\text{rad}}(T_R)$ . Using this criteria, the total energy density at any temperature  $T$  reads [11, 12]

$$\rho(T) = \rho_{\text{rad}}(T) + \rho_\varphi(T) \quad (3)$$

$$= \rho_{\text{rad}}(T) \left[ 1 + \frac{g_*(T_R)}{g_*(T)} \left( \frac{g_{*s}(T)}{g_{*s}(T_R)} \right)^{(4+n)/3} \left( \frac{T}{T_R} \right)^n \right] \quad (4)$$

Now, from standard Friedman equation one can write the Hubble parameter in terms of the energy density as

$$\mathcal{H} = \frac{\sqrt{\rho}}{\sqrt{3}M_{\text{Pl}}}, \quad (5)$$

with  $M_{\text{Pl}} = (8\pi G)^{-1/2} = 2.4 \times 10^{18}$  GeV being the reduced Planck mass. At temperature higher than  $T_R$  with the condition  $g_*(T) = \bar{g}_*$  which can be considered to be some constant, the Hubble rate can approximately be recasted as [11]

$$\begin{aligned} \mathcal{H}(T) &= \mathcal{H}_R(T) \left[ 1 + \left( \frac{T}{T_R} \right)^n \right]^{1/2} \\ &\approx \frac{\pi \bar{g}_*^{1/2}}{3\sqrt{10}} \frac{T^2}{M_{\text{Pl}}} \left( \frac{T}{T_R} \right)^{n/2}, \quad (T \gg T_R), \end{aligned} \quad (6)$$

where  $H_R(T)$  is the Hubble parameter in the standard radiation dominated universe. In case of SM  $\bar{g}_* \equiv g_*(\text{SM}) = 106.75$ . It is important to note from Eq. (6) that the expansion rate is larger than what it is supposed to be in the standard cosmological background for  $T > T_R$  and  $n > 0$ . It is noteworthy that  $T_R$  can not be too small such that it changes the standard BBN history. For a certain value of  $n$ , BBN constraints provide a lower limit on  $T_R$  [11]:

$$T_R \gtrsim (15.4)^{1/n} \text{ MeV}. \quad (7)$$

As one can see, for larger  $n$  this constraint becomes more and more loose. Before moving on to the next section we would like to comment that in order to get values larger than  $n = 2$ , a negative scalar potential is to be considered. A specific structure of  $n > 2$  potential can be found in [11, 21] which is asymptotically free.

<sup>1</sup>GW signal in a modified cosmological scenario have also been studied in details in [18–20]

### III. DARK MATTER YIELD VIA FREEZE-IN

In this section we will discuss the modification of standard Boltzmann equation [10] governing the DM number density due to the effect of fast expansion encoded in the Hubble parameter  $\mathcal{H}$  (Eq. (6)). The key for freeze-in [22, 23] DM production is to assume that DM was not present in the early universe. The DM is then produced via annihilation and/or decay of the particles in the thermal bath. Due to the extremely feeble coupling of the DM with the visible sector particles the DM never really enters into thermal equilibrium. Now, the Boltzmann equation (BEQ) for DM production via annihilation for  $2 \rightarrow 2$  processes of the form  $a, b \rightarrow 1, 2$  is then given by [24]:

$$\dot{n}_1 + 3\mathcal{H}n_1 = \int d\Pi_1 d\Pi_2 d\Pi_a d\Pi_b (2\pi)^4 \delta^4(p_1 + p_2 - p_a - p_b) |\mathcal{M}|_{a,b \rightarrow 1,2}^2 f_a f_b, \quad (8)$$

where  $d\Pi_j = \frac{d^3 p_j}{2E_j (2\pi)^3}$  are Lorentz invariant phase space elements, and  $f_i$  is the phase space density of particle  $i$  with corresponding number density being:

$$n_i = \frac{g_i}{(2\pi)^3} \int d^3 p f_i, \quad (9)$$

with  $g_i$  is the internal degrees of freedom (DOF). Here we have made two crucial assumptions: the initial abundance for particle 1 is negligible such that  $f_1 \approx 0$  and we also neglect Pauli-blocking/stimulated emission effects, i.e. approximating  $1 \pm f_i \approx 1$ . The BEQ in Eq. (8) can be rewritten as an integral with respect to the CM energy as [13, 22]:

$$\dot{n}_1 + 3\mathcal{H}n_1 \approx \frac{T}{512\pi^6} \int_{s=4m_\chi^2}^{\infty} ds d\Omega P_{ab} P_{12} |\mathcal{M}|_{ab \rightarrow 12}^2 \frac{1}{\sqrt{s}} K_1 \left( \frac{\sqrt{s}}{T} \right), \quad (10)$$

where  $P_{ij} = \frac{1}{2\sqrt{s}} \sqrt{s - (m_i + m_j)^2} \sqrt{s - (m_i - m_j)^2} \rightarrow \frac{\sqrt{s}}{2}$  in the limit  $m_{i,j} \rightarrow 0$ . The BEQ in terms of the yield  $Y_\chi = n_1/s$  can be written in the differential form as:

$$-s(T) \cdot \mathcal{H}(T) \cdot T \cdot \frac{dY_\chi^{\text{ann}}}{dT} = \frac{T}{512\pi^6} \int_{s=4m_\chi^2}^{\infty} ds d\Omega P_{ab} P_{12} |\mathcal{M}|_{ab \rightarrow 12}^2 \frac{1}{\sqrt{s}} K_1 \left( \frac{\sqrt{s}}{T} \right). \quad (11)$$

The total yield due then turns out to be:

$$Y_\chi(T) = \frac{1}{512\pi^6} \int_T^{T_{\text{max}}} \frac{dT'}{s(T') \cdot \mathcal{H}(T')} \int_{s=4m_\chi^2}^{\infty} ds d\Omega \left( \frac{\sqrt{s}}{2} \right)^2 |\mathcal{M}|_{ab \rightarrow 12}^2 \frac{1}{\sqrt{s}} K_1 \left( \frac{\sqrt{s}}{T'} \right) \quad (12)$$

where we have put  $m_{i,j} = 0$  just for convenience. The upper limit of the  $T$  integration is considered to be  $T_{\text{max}} = T_{\text{RH}}$  corresponding to the reheat temperature of the universe. Eq. (12) should be divided into two eras: one before EWSB with  $T > 160$  GeV and the other post-EWSB for  $T \lesssim 160$  GeV. For  $T_{\text{RH}} \gg T_{\text{EW}}$  the DM production is dominant before EWSB. The lower limit on the  $s$  integral can be approximated to zero if the DM mass is negligible compared to reheat temperature of the universe. For a lower reheat temperature, however, one can not ignore the masses of the particle spectrum in the theory and for  $T_{\text{RH}} \sim m_i$  the IR nature of the yield becomes prominent [25]. Since in a fast expanding universe the Hubble parameter gets modified according to Eq. (6), the resulting DM yield also gets affected following Eq. (12). In the next section we shall quantify this through analytical and numerical computation. Finally, the relic abundance of the DM at present temperature can be obtained via:

$$\Omega_{\text{DM}} h^2 = (2.75 \times 10^8) \frac{m_{\text{DM}}}{\text{GeV}} Y_{\text{DM}}^{\text{total}}(T_0), \quad (13)$$

where we find  $Y_{\text{DM}}^{\text{total}}(T_0)$  by solving Eq. (12) numerically. The important point here to note is that due to modified Hubble rate  $\mathcal{H}$  the DM yield and consequently the DM abundance is now a function of the fast expansion parameters  $n, T_R$  on top of DM mass, reheat temperature and the effective scale.

#### A. A toy model

We consider a minimal dark sector comprising of a Dirac fermion singlet  $\chi$  and a scalar singlet  $\phi$ . There exists a  $Z_4$  symmetry under which only the dark sector particles are charged as tabulated in Tab. I. We assume the fermion  $\chi$  to be the lightest particle charged under the new symmetry and hence a potential DM candidate. With this symmetry assigned one can then write the effective Lagrangian for the dark sector as:

Symmetry	$\chi$	$\phi$
$Z_4$	i	-1

Table I. Transformation of the new particles under  $Z_4$  symmetry.

$$\mathcal{L} \supset \bar{\chi} (i\cancel{\partial} - m_\chi) \chi - y_\chi \bar{\chi}^c \chi \phi + \frac{1}{\Lambda} \bar{\chi} \chi |H|^2 - V(H, \phi) \quad (14)$$

with the renormalizable scalar potential given by

$$V(H, \phi) \supset -\mu_H^2 |H|^2 + \mu_\phi^2 \phi^2 + \lambda_H |H|^4 + \lambda_\phi \phi^4 + \lambda_{H\phi} |H|^2 \phi^2. \quad (15)$$

The  $Z_4$  symmetry prevents us from writing any odd terms in the scalar potential. Note that the portal coupling  $\lambda_{H\phi} \sim \mathcal{O}(1)$  keeps the singlet scalar  $\phi$  in equilibrium with the thermal bath. As the new singlet scalar  $\phi$  does not acquire any non-zero VEV,  $\chi$  has only a pure Dirac mass term  $m_\chi$ . Because of the  $Z_4$  symmetry it is also not possible to write Majorana mass terms for  $\chi$  that otherwise would have resulted in a pseudo-Dirac splitting [26]. The second term in Eq. (14), due to its renormalizable nature, contributes to the DM abundance via Infra-Red (IR) freeze-in due to  $\phi \rightarrow \chi\chi$  decay which is kinematically accessible as long as  $m_\chi < m_\phi/2$ . The third term shall contribute to UV freeze-in [13] for DM production via  $HH \rightarrow \chi\chi$  contact interaction before EWSB while after EWSB one can have both UV and IR freeze-in contribution due to non-zero VEV of the Higgs that results in renormalizable DM-SM interaction. For UV freeze-in the abundance is sensitive to the maximum temperature of the thermal bath, which we assume to be the reheat temperature  $T_{\text{RH}}$ <sup>2</sup>. This is in sharp contrast to the IR freeze-in scenario where the two sectors communicate via renormalizable operators, and the DM abundance is set by the IR physics *i.e.*, the yield becomes maximum at low temperature, typically at  $T \sim m_{\text{DM}}$  [22, 23]. Now, the reheat temperature  $T_{\text{RH}}$  of the universe is somewhat loosely bounded. Typically, the lower bound on  $T_{\text{RH}}$  comes from the measurement of light element abundance during BBN, which requires  $T_{\text{RH}} \gtrsim 4.7$  MeV. The upper bound, on the other hand, may emerge from (i) cosmological gravitino problem [28, 29] in the context of supersymmetric framework, that demands  $T_{\text{RH}} \lesssim 10^{10}$  GeV to prohibit thermal gravitino over production and (ii) simple inflationary scenarios that require at most  $T_{\text{RH}} \sim 10^{16}$  GeV [30, 31] for a successful inflation. In view of this, the maximum reheat temperature of the universe can be regarded as a free parameter.

## B. Relic abundance of the dark matter

A model-independent study of IR freeze-in in context of fast expansion has been done in [12]. Here we would like to see the effect of such fast expansion in the context of pure UV freeze-in before electroweak symmetry breaking, together with IR freeze-in, once the electroweak symmetry is broken. The requirement of obtaining right DM relic abundance via UV freeze-in shall also put some bound on the reheat temperature, along with the cut-off scale  $\Lambda$  of the theory in the fast expanding scenario. Up to this end we note that the contribution to DM abundance via IR freeze-in through  $\phi \rightarrow \chi\chi$  is negligible once

we choose the Yukawa coupling  $y_\chi \lesssim 10^{-12}$ <sup>3</sup>. Such a choice of coupling might look like somewhat “fine-tuned” but the smallness of coupling for IR freeze-in is in itself a requirement to keep the DM out of thermal equilibrium. The small Yukawa coupling thus prevents the dark sector to reach thermal equilibrium within itself without hampering the rest of our analysis. This makes UV freeze-in as the dominant process that can produce the total observed DM relic via decay and /or annihilation which we will discuss below.

In order to calculate the DM relic abundance by solving Eq. (12) we first point out the possible annihilation and decay channels leading to DM pair production above and below the electroweak symmetry breaking temperature  $T \simeq 160$  GeV. Before EWSB *i.e.*,  $T > 160$  GeV, for the  $SU(2)_L$  scalar doublet, the propagating DOFs are the Goldstone bosons (GB):

$$H = \begin{pmatrix} \varphi^+ \\ \varphi^0 \end{pmatrix}, \quad (16)$$

which are then converted to the longitudinal DOF for the massive gauge bosons after EWSB in unitary gauge:

$$H = \begin{pmatrix} 0 \\ \frac{h+v_h}{\sqrt{2}} \end{pmatrix},$$

where  $h$  is the CP-even SM-like Higgs field. After electroweak symmetry breaking (EWSB) *i.e.*,  $T \lesssim 160$  GeV there can be several  $2 \rightarrow 2$  annihilation channels (mediated by SM Higgs) that can produce the DM via freeze-in, while the  $1 \rightarrow 2$  decay channels will only contribute if  $m_h > 2m_\chi$  (see Fig. 1). Another SM Higgs mediated  $2 \rightarrow 2$  process is shown in bottom left of Fig. 1 with the non-standard scalars  $\phi$  in the initial state. The amplitude for this process goes roughly as  $\lambda_{H\phi}^2 v_h^4 / \Lambda^2$ . For  $\lambda_{H\phi} \lesssim \mathcal{O}(1)$  and  $\Lambda \gtrsim \mathcal{O}(10^8)$  GeV, however, this process has negligible contribution to the DM yield via IR freeze-in. Using Eq. (12) it is possible to derive an approximate analytical expression for DM yield via UV freeze-in (before EWSB). As all the SM particles are also massless before EWSB, the squared amplitude for the 4-point processes simply become

$$|\mathcal{M}|^2 \simeq \frac{s}{\Lambda^2}. \quad (17)$$

Considering the DM and  $\phi$  mass to be negligible compared to  $\{\Lambda, T_{\text{RH}}\}$ , for  $T \gg T_R$ , we can analytically obtain the expression for DM yield before EWSB

<sup>2</sup>In principle, the maximum temperature during reheating can be larger than  $T_{\text{RH}}$  [27].

<sup>3</sup>For example, for DM mass of 20 GeV and  $m_\phi = 70$  GeV choosing  $y_\chi = 10^{-12}$  gives rise to DM relic abundance of  $\sim 10^{-3}$  dominantly via  $\phi \rightarrow \chi\chi$  decay with a lifetime of  $\sim 0.4$  sec.



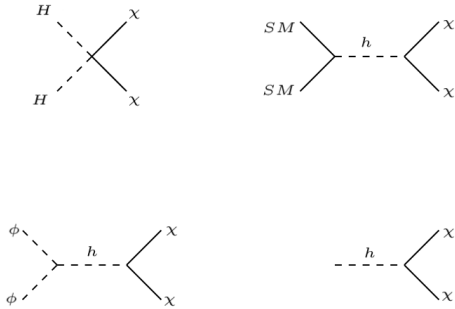


Figure 1. DM yield via freeze-in before EWSB (top left) and after EWSB (top right and bottom). Here SM stands for all the SM gauge bosons, quarks and leptons. Here  $H$  stands for the SM-like Higgs field before EWSB and  $h$  is the CP-even Higgs field after EWSB.

$$Y_\chi = \begin{cases} \xi \left( \frac{T_R}{T_{EW}} \right)^{n/2} \frac{T_{EW}}{\Lambda^{2(n-2)}} \left[ 1 - \frac{T_{RH}}{T_{EW}} \left( \frac{T_{EW}}{T_{RH}} \right)^{n/2} \right], & (n \neq 2) \\ \frac{\xi T_R}{2\Lambda^2} \log \left[ \frac{T_{RH}}{T_{EW}} \right] & (n = 2) \end{cases} \quad (18)$$

where  $\xi = \frac{45M_{pl}}{1696\sqrt{106}\pi^8}$  is a constant of mass dimension unity. After EWSB there will be IR dominated processes as well which are proportional to  $(v/\Lambda)^2$ . Now, since all the SM particles become massive after EWSB (together with the DM), hence one has to find the DM yield numerically in this regime. The only possible decay channel contributing to DM abundance is  $h \rightarrow \chi\chi$  which is available if  $m_\chi < m_h/2$ . We can obtain an approximate analytical expression for the yield due to decay [12] as

$$\begin{aligned} Y_\chi^{\text{decay}} &= \int_{T_{\min}}^{T_{\max}} dT \frac{m_h^2 \Gamma_{h \rightarrow \chi\chi}}{2\pi^2} \frac{K_1(m_h/T)}{s(T) \mathcal{H}(T)} \\ &\approx \frac{\Gamma_{h \rightarrow \chi\chi} T_R^{n/2}}{2\pi^2 m_h^{\frac{n}{2}+2}} \frac{M_{pl}}{A} \int_0^\infty dx x^{3+n/2} K_1(x) \\ &= \frac{2M_{pl} \Gamma_{h \rightarrow \chi\chi}}{A\pi^2 m_h^2} \left( \frac{T_R}{m_h} \right)^{n/2} \left[ 2^{n/2} \Gamma\left(\frac{6+n}{4}\right) \Gamma\left(\frac{10+n}{4}\right) \right], \end{aligned} \quad (19)$$

where  $A$  contains all the dimensionless constants and we assumed  $T_{\max} \rightarrow \infty$  (which, in reality, should be  $T_{EW}$ ) such that  $x_{\max} \rightarrow 0$  with  $T_{\min} = 0$ . The decay width goes roughly as  $\Gamma_{h \rightarrow \chi\chi} \propto (v/\Lambda)^2$ . In the case of  $2 \rightarrow 2$  annihilation processes, in the limit where all the SM particles are massless, the analytical form of the yield after EWSB turns out to be

$$Y_\chi^{2 \rightarrow 2} \sim \frac{m_\chi M_{pl}}{B\Lambda^2} \left( \frac{T_R}{m_\chi} \right)^{n/2} \int_{x_{\min}}^{x_{\max}} dx x^{n/2-2}, \quad (20)$$

with  $x_{\max} = m_\chi/T_0$  and  $x_{\min} = m_\chi/T_{EW}$ , where  $B$  contains all the dimensionless constants. Taking all the masses of the particles into account, however, such a simple analytical expression would be difficult to obtain and one has to resort to numerical computation. The asymptotic nature of the yield after EWSB can be determined from Eq. (19) and Eq. (20) which tells that the yield is suppressed for larger  $n$  as  $x \rightarrow \infty$ . Under the framework of faster expansion one can not vary  $T_{RH}$ ,  $T_R$  and  $n$  arbitrarily as pointed out in [12]. The dominance of  $\rho_\phi$  at early universe sets an upper bound on the reheat temperature since beyond  $\rho_\phi \sim M_{pl}^4$  this framework fails. This, together with Eq. (6), sets an upper bound on the reheat temperature [12]

$$\begin{aligned} H &\sim \frac{T^2}{M_{pl}} \left( T_{RH}/T_R \right)^{n/2} \lesssim M_{pl} \\ \implies T_{RH} &\lesssim M_{pl} \left( M_{pl}^{-1} T_R \right)^{n/n+4}. \end{aligned} \quad (21)$$

Note that the above bound gets stronger for larger  $n$ . Additionally, for the effective theory to remain valid  $\Lambda > m_\chi$ ,  $T_{RH}$  is mandatory. For processes appearing before and after EWSB we compute the DM yield by performing numerical integrations using *Mathematica*. In Fig. 2 we have illustrated how the DM yield varies with  $x = m_\chi/T$  for a fixed  $T_R = 40$  MeV and reheat temperature  $T_{RH} = 10^8$  GeV for different choices of  $n$ -values for different DM masses  $m_\chi = \{50, 500\}$  GeV. For all these plots we have kept  $T_{RH} = 10^8$  GeV which implies  $n \lesssim 4$  following Eq. (21). First of all we see all these curves converge as  $x \rightarrow \infty$  since all of them satisfy the DM relic abundance for a fixed DM mass of 50 GeV (on left panel) and 500 GeV (on right panel). Also note that the DM yield builds up very early at a smaller  $x$  ( $T \sim T_{RH}$ ) which is the typical feature of UV freeze-in when  $T_{RH} \gg m$  [13, 25]. For larger  $n$ , as one can notice from Eq. (12), the DM yield gets suppressed since  $\mathcal{H}$  becomes larger according to Eq. (6) for a fixed  $T_{RH}$ . This shows that the freeze-in production of DM in a fast expanding universe is dramatically suppressed which has also been reported earlier [12]. Thus, a larger  $n$  requires a smaller  $\Lambda$  to achieve right DM abundance for a fixed  $T_{RH}$  as  $Y_\chi \propto \frac{1}{\Lambda^2}$ . The orange curves ( $n = 4$ ) in Fig. 2 correspond to  $\Lambda \sim 10^9$  GeV which is about five orders less than that for the red curves (standard case) corresponding to which  $\Lambda \sim 10^{15}$  GeV. This exactly what is reflected in Fig. 3 where we show DM abundance satisfying contours in  $\Lambda$ - $T_{RH}$  plane for DM mass of  $m_\chi = \{50, 500\}$  GeV in the left and in the right panel respectively considering all processes appearing before and after EWSB. For a 50 GeV DM  $h \rightarrow \chi\chi$  decay contributes significantly after EWSB via IR freeze-in [32]. As a result we see the horizontal part in the red and green curves for  $T_{RH} \lesssim 10$  TeV. This arises due to the IR nature of the freeze-in where the DM abundance depends no more on the reheat temperature, rather on the mass of the decaying mother particle (which is Higgs in this case). For larger  $n$  although the

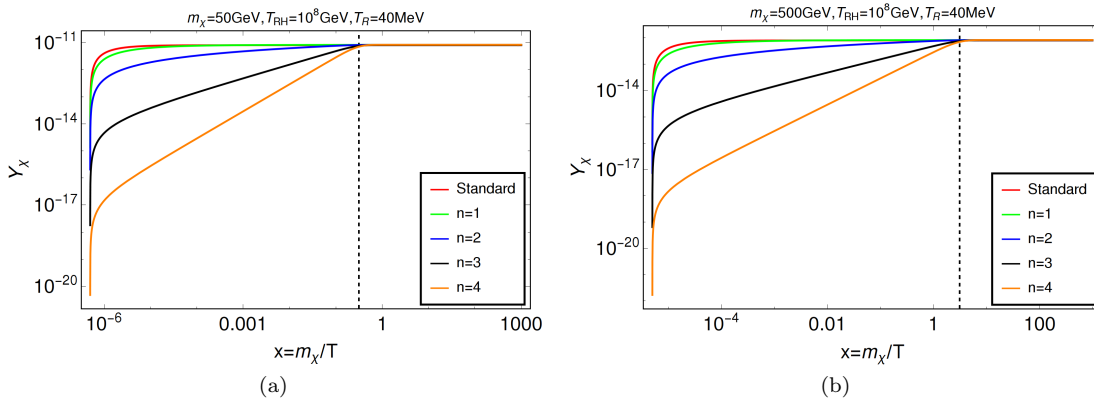


Figure 2. (a): Variation of DM yield  $Y_\chi$  with  $x = m_\chi/T$  for different values of  $n = \{1, 2, 3, 4\}$  shown in green, blue, black and orange respectively for  $m_\chi = 50$  GeV,  $T_{RH} = 10^8$  GeV and  $T_R = 40$  MeV. Each curve satisfies observed relic abundance for different values of the cut-off scale  $\Lambda \approx \{10^{15}, 10^{13}, 10^{11}, 10^{10}\}$  GeV respectively. (b): Same as (a) for  $m_\chi = 500$  GeV. The dashed black straight line in both plots corresponds to  $x_{EW} = m_\chi/T_{EW}$ .

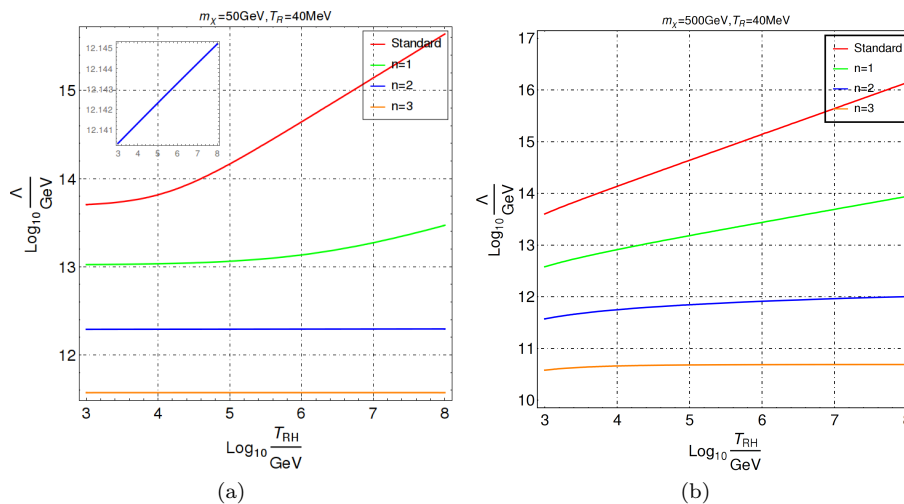


Figure 3. (a): Contours satisfying PLANCK observed relic abundance in the bi-dimensional plane of  $\Lambda$ - $T_{RH}$  for different choices of  $n = \{1, 2, 3\}$  shown in green, blue and orange respectively where the DM mass is fixed at 50 GeV and  $T_R = 40$  MeV. (b): Same as (a) for  $m_\chi = 500$  GeV.

curves look absolutely flat (*e.g.*, the blue one) but as one can see from the inset figure their variation over  $\Lambda$  is almost negligible compared to the standard case or  $n = 1$  case. For a heavier DM mass, typically  $m_\chi \gg T_{EW}$ , most of the contribution to the DM yield comes from processes before EWSB. As a consequence we observe typical UV nature in the contours on the right panel of Fig. 3 where the cut-off scale rises linearly with the reheat temperature. For small enough  $T_{RH} \ll 1$  TeV the IR nature of the freeze-in might show up even for heavier DM but we choose to confine ourselves to  $T_{RH} \gtrsim 1$  TeV.

We conclude this section by inferring that one has to increase the effective dimensionful coupling  $\propto \Lambda^{-1}$  with respect to the standard cosmological background in order to get the right DM abundance in a fast expanding background. This implies that for non-renormalizable in-

teractions with dimension larger than five, it is possible to bring down  $\Lambda \sim \text{TeV}$  for  $n > 0$  that provides larger detection prospect for UV freeze-in. For dimension five interactions, since for larger  $n$  the DM yield gets more and more suppressed, hence we stick only up to  $n = 4$ . For such a choice of  $n$ , as we have illustrated, it is possible to obtain observed DM relic abundance for different choices of  $T_R$  and  $T_{RH}$  obeying Eq. (7) and Eq. (21) by suitably modifying the cut-off scale  $\Lambda$ . As we shall see in the next section, for such a choice of  $n$ ,  $T_R$  it is possible to generate a strong first order phase transition that is capable of explaining the NANOGrav 12.5 yrs data.

#### IV. STOCHASTIC GRAVITATIONAL WAVE SIGNAL IN A FAST EXPANDING UNIVERSE

In general, an extended scalar sector may give rise to a strong first order phase transition (SFOPT) resulting in stochastic gravitational wave (GW) with detectable frequencies (see, for example [33]). In our case the presence of an extra scalar singlet  $\phi$  does that job. In the context of the present model we would like to explore how the frequency and amplitude of such a stochastic GW signal can get modified due to the fast expansion of the universe. Our particular interest is to explore if a simple dark sector can explain the NANOGrav data when the cosmological background is modified. As we shall see, the stochastic GW signal that can explain the reported NANOGrav data [1] can only be generated in a fast expanding universe for some specific choices of  $T_R, n$ .

##### 1. Finite Temperature Effective Potential

To construct the finite temperature effective potential, we add two temperature corrected terms with the tree-level potential. The effective potential at a finite temperature  $T$  then can be written as [34]

$$V_{\text{eff}} = V_{\text{tree-level}} + V_{1\text{-loop}}^{T=0} + V_{1\text{-loop}}^{T \neq 0}, \quad (22)$$

where  $V_{\text{tree-level}}$ ,  $V_{1\text{-loop}}^{T=0}$  and  $V_{1\text{-loop}}^{T \neq 0}$  are the zero temperature tree level potential, zero temperature Coleman-Weinberg (CW) one-loop potential and the finite temperature one-loop potential respectively. As mentioned earlier, the scalar sector under consideration contains a real scalar singlet on top of the SM-like Higgs doublet which leads to Eq. (15). The SM Higgs  $H$  can be represented as

$$H = \begin{pmatrix} G^+ \\ \frac{1}{\sqrt{2}}(v + h + iG^0) \end{pmatrix}, \quad (23)$$

where  $G^+$  and  $G_0$  are the charged and the neutral Goldstone bosons after the spontaneous symmetry breaking. To explore the electroweak phase transition we replace the scalar fields  $H$  and  $\phi$  with their VEVs  $v, v_\phi$  respectively. Now Eq. (15) can be expressed as

$$V_{\text{tree-level}}^{T=0} = -\frac{1}{2}\mu_H^2 v^2 + \frac{1}{2}\mu_\phi^2 v_\phi^2 + \frac{1}{4}\lambda_H v^4 + \frac{1}{4}\lambda_\phi v_\phi^4 + \frac{1}{4}\lambda_{H\phi} v^2 v_\phi^2. \quad (24)$$

Note that, although the scalar  $\phi$  do not acquire any vacuum expectation value (VEV) at  $T = 0$  (to keep the  $Z_2$  symmetry intact), but its VEV can be generated at a finite temperature. Here the classical VEVs  $v, v_\phi$  change with temperature *i.e.*, behave like a field and at

the zero temperature it tends to the classical fixed values. The zero-temperature CW one-loop effective potential is given by [34, 35]

$$V_{1\text{-loop}}^{T=0} = \pm \frac{1}{64\pi^2} \sum_i n_i m_i^4 \left[ \log \frac{m_i^2}{Q^2} - C_i \right], \quad (25)$$

where the '+' and '-' symbols appear due to bosons and fermions respectively. The quantity  $Q$  denotes the renormalization scale which we take  $Q = v = 246.22$  GeV in our work. The summation  $i$  is over all the particle species associated in the scalar potential with  $i \in (h, \phi, G^\pm, G^0, W, Z, t)$ . In Eq. (25), the quantities  $n_i$ ,  $m_i$  and  $C_i$  represents the number of degrees of freedom, the field-dependent masses and renormalization-scheme-dependent numerical constant of the  $i$ th particle species respectively. The associated degrees of freedom of the particles are  $(n_{W^\pm})_L = 4$ ,  $(n_{W^\pm})_T = 2$ ,  $(n_Z)_L = 2$ ,  $(n_Z)_T = 1$ ,  $n_t = 12$ ,  $n_{G^\pm} = 2$  and  $n_{h, \phi, G^0} = 1$ . The values of the renormalization-scheme-dependent constant  $C_i$  are  $(C_{W,Z})_T = 1/2$  for the transverse component of  $W, Z$  boson,  $(C_{W,Z})_L = 3/2$  for the longitudinal component of  $W, Z$  boson and for the other particles,  $C_{h, \phi, G^+, G^-, G^0, t} = 3/2$ . We perform our calculations by considering the Landau gauge where the Goldstone bosons are massless at  $T = 0$  and also the theory is free from ghost contributions [36]. With this, the finite temperature one-loop effective potential can be expressed as [34]

$$V_{1\text{-loop}}^{T \neq 0} = \frac{T^4}{2\pi^2} \sum_i n_i J_\pm \left[ \frac{m_i^2}{T^2} \right], \quad (26)$$

where

$$J_\pm \left( \frac{m_i^2}{T^2} \right) = \pm \int_0^\infty dy y^2 \log \left( 1 \mp e^{-\sqrt{y^2 + \frac{m_i^2}{T^2}}} \right). \quad (27)$$

We include the thermal correction to the boson masses by applying daisy resummation method [37] as  $\mu_H^2(T) = \mu_H^2 + c_1 T^2$  and  $\mu_\phi^2(T) = \mu_\phi^2 + c_2 T^2$  where

$$c_1 = \frac{6\lambda_H + 2\lambda_{H\phi}}{12} + \frac{3g^2 + g'^2}{16} + \frac{y_t^2}{4} \quad (28)$$

and

$$c_2 = \frac{6\lambda_\phi + 2\lambda_{H\phi}}{12}, \quad (29)$$

with the couplings  $g, g'$  and  $y_t$  as the  $SU(2)_L$  gauge coupling,  $U(1)_Y$  gauge coupling and top Yukawa coupling of the SM respectively. We also include the thermal corrections to the  $W$  and  $Z$  boson masses with the modified thermal masses [36]

$$m_W^2(T) = \frac{1}{4}g^2v^2 + 2g^2T^2, \quad (30)$$

and

$$m_Z^2(T) = \frac{1}{8}(g^2 + g'^2)v^2 + (g^2 + g'^2)T^2 + \frac{1}{8}\sqrt{[(g^2 - g'^2)^2(64T^2 + 16T^2v^2) + (g^2 + g'^2)^2v^4]}. \quad (31)$$

With this set-up we then proceed to analyze the GW production due to strong first order phase transition (SFOPT).

## 2. Gravitational wave production from SFOPT

Here we discuss the possible production mechanism of GW from the strong first-order electroweak phase transition originating mainly via bubble collisions [38–44], sound waves induced by the bubbles running through the cosmic plasma [45–48] and turbulence induced by the bubble expansions in the cosmic plasma [49–53]. The total GW intensity  $\Omega_{\text{GWh}^2}$  for a particular frequency  $f$  can be estimated by considering the contributions of the above three processes and can be expressed as [38–55]

$$\Omega_{\text{GWh}^2} = \Omega_{\text{colh}^2} + \Omega_{\text{SWh}^2} + \Omega_{\text{turh}^2}. \quad (32)$$

The expression for the GW intensity from the component of bubbles collision  $\Omega_{\text{colh}^2}$  is given by

$$\Omega_{\text{colh}^2} = 1.67 \times 10^{-5} \left(\frac{\beta}{\mathcal{H}}\right)^{-2} \frac{0.11v_w^3}{0.42 + v_w^2} \left(\frac{\kappa\alpha}{1+\alpha}\right)^2 \left(\frac{g_*}{100}\right)^{-\frac{1}{3}} \frac{3.8\left(\frac{f}{f_{\text{col}}}\right)^{2.8}}{1 + 2.8\left(\frac{f}{f_{\text{col}}}\right)^{3.8}}, \quad (33)$$

where the parameter  $\beta$  has the form

$$\beta = \left[ \mathcal{H}T \frac{d}{dT} \left( \frac{S_3}{T} \right) \right] \Big|_{T_n}, \quad (34)$$

where  $S_3(T)$  is the Euclidean action of the critical bubble. In general, the nucleation of the bubbles occur at a temperature  $T_n$  where the condition  $S_3(T_n)/T_n \approx 140$  [34] is satisfied. In Eq. (34)  $\mathcal{H}$  denotes the Hubble parameter at the nucleation temperature  $T_n$  which is given by Eq. (6) for the fast expanding universe. The bubble wall velocity  $v_w$  is computed using the most general expression for the wall velocity [39, 43, 56, 57]

$$v_w = \frac{1/\sqrt{3} + \sqrt{\alpha^2 + 2\alpha/3}}{1 + \alpha}. \quad (35)$$

The quantity  $\kappa$  in Eq. (33) is given by

$$\kappa = 1 - \frac{\alpha_\infty}{\alpha}, \quad (36)$$

with [58, 59]

$$\alpha_\infty = \frac{30}{24\pi^2 g_*} \left(\frac{v_n}{T_n}\right)^2 \left[ 6\left(\frac{m_W}{v}\right)^2 + 3\left(\frac{m_Z}{v}\right)^2 + 6\left(\frac{m_t}{v}\right)^2 \right]. \quad (37)$$

where  $v_n$  is the Higgs VEV at the nucleation temperature  $T_n$ ,  $m_W$ ,  $m_Z$  and  $m_t$  are the masses of the gauge bosons  $W$ ,  $Z$  and the top quark  $t$  respectively. The phase transition parameter  $\alpha$  can be expressed as

$$\alpha = \left[ \frac{\rho_{\text{vac}}}{\rho_{\text{rad}}^*} \right] \Big|_{T_n}. \quad (38)$$

where  $\rho_{\text{rad}}^*$  is the background energy density of the plasma and  $\rho_{\text{vac}}$  is the energy density difference between false and true vacuum during the electroweak phase transition. The quantities  $\rho_{\text{vac}}$  and  $\rho_{\text{rad}}^*$  have the following form

$$\rho_{\text{vac}} = \left[ \left( V_{\text{eff}}^{\text{high}} - T \frac{dV_{\text{eff}}^{\text{high}}}{dT} \right) - \left( V_{\text{eff}}^{\text{low}} - T \frac{dV_{\text{eff}}^{\text{low}}}{dT} \right) \right] \quad (39)$$

and

$$\rho_{\text{rad}}^* = \frac{g_* \pi^2 T_n^4}{30}. \quad (40)$$

In Eq. (33) the peak frequency  $f_{\text{col}}$  from the bubble collisions is given by

$$f_{\text{col}} = 16.5 \times 10^{-6} \text{ Hz} \left( \frac{0.62}{v_w^2 - 0.1v_w + 1.8} \right) \left( \frac{\beta}{\mathcal{H}} \right) \left( \frac{T_n}{100 \text{ GeV}} \right) \left( \frac{g_*}{100} \right)^{\frac{1}{6}}. \quad (41)$$

Next, the expression for GW intensity from the component of sound wave (SW) is given by



$$\Omega_{\text{SW}} h^2 = 2.65 \times 10^{-6} \left(\frac{\beta}{\mathcal{H}}\right)^{-1} v_w \left(\frac{\kappa_v \alpha}{1 + \alpha}\right)^2 \left(\frac{g_*}{100}\right)^{-\frac{1}{3}} \left(\frac{f}{f_{\text{SW}}}\right)^3 \left[\frac{7}{4 + 3 \left(\frac{f}{f_{\text{SW}}}\right)^2}\right]^{\frac{7}{2}}, \quad (42)$$

where the parameter  $\kappa_v$

$$\kappa_v = \frac{\alpha_\infty}{\alpha} \left[ \frac{\alpha_\infty}{0.73 + 0.083\sqrt{\alpha_\infty + \alpha_\infty}} \right]. \quad (43)$$

The peak frequency  $f_{\text{SW}}$  from the sound wave contribution reads

$$f_{\text{SW}} = 1.9 \times 10^{-5} \text{ Hz} \left(\frac{1}{v_w}\right) \left(\frac{\beta}{\mathcal{H}}\right) \left(\frac{T_n}{100 \text{ GeV}}\right) \left(\frac{g_*}{100}\right)^{\frac{1}{44}}$$

For the contribution of SW to the total GW intensity depends on the Hubble time scale. If it survives more than a Hubble time then the expression in Eq. (42) will be valid, otherwise we need to include a factor called *suppression factor* to the SW component of the GW intensity. Following [59–61] we compute the suppression factor  $\frac{\mathcal{H} R_*}{\bar{U}_f}$  (where  $\bar{U}_f$  is the root-mean-square (RMS) fluid velocity and  $R_*$  is the mean bubble separation) to check whether the SW components lasts more than a Hubble time.

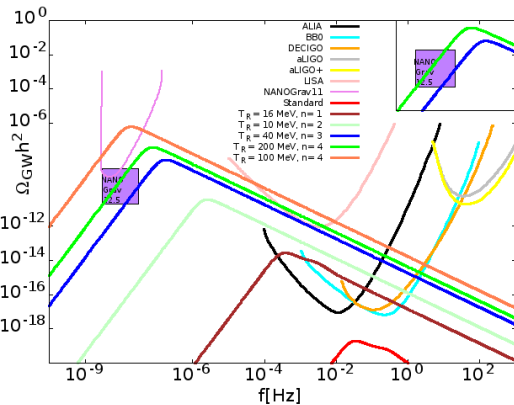


Figure 4. Plot of calculated GW intensities as a function of frequency for different choices of  $\{n, T_R\}$ . The sensitivity curves of NANOGrav11, NANOGrav12.5 (purple coloured rectangular box), future GW detectors such as ALIA, BBO, DECIGO, LISA, aLIGO and aLIGO+ are also shown in the same plane.

Lastly, the expression for GW intensity from the turbulence in the plasma  $\Omega_{\text{turb}} h^2$  is given by

$$\Omega_{\text{turb}} h^2 = 3.35 \times 10^{-4} \left(\frac{\beta}{\mathcal{H}}\right)^{-1} v_w \left(\frac{\epsilon \kappa_v \alpha}{1 + \alpha}\right)^{\frac{3}{2}} \left(\frac{g_*}{100}\right)^{-\frac{1}{3}} \frac{\left(\frac{f}{f_{\text{turb}}}\right)^3 \left(1 + \frac{f}{f_{\text{turb}}}\right)^{-\frac{11}{3}}}{\left(1 + \frac{8\pi f}{h_*}\right)}, \quad (45)$$

with

$$h_* = 16.5 \times 10^{-6} \text{ Hz} \left(\frac{T_n}{100 \text{ GeV}}\right) \left(\frac{g_*}{100}\right)^{\frac{1}{6}}. \quad (46)$$

Here  $\epsilon = 0.1$  and the peak frequency  $f_{\text{turb}}$  from the turbulence mechanism has the form

$$f_{\text{turb}} = 2.7 \times 10^{-5} \text{ Hz} \left(\frac{1}{v_w}\right) \left(\frac{\beta}{\mathcal{H}}\right) \left(\frac{T_n}{100 \text{ GeV}}\right) \left(\frac{g_*}{100}\right)^{\frac{1}{47}}$$

BP	$m_h$ in GeV	$m_\phi$ in GeV	$\lambda_H$	$\lambda_\phi$	$\lambda_{H\phi}$
1	125.09	70	0.129	0.1	0.1

Table II. Chosen benchmark point to demonstrate strong first-order phase transition.

BP	$v_c$ in GeV	$T_c$ in GeV	$\frac{v_c}{T_c}$	$v_n$ in GeV	$T_n$ in GeV	$\alpha$
1	140.50	134	1.04	151.20	134.58	0.0028

Table III. Values of thermal parameters for the chosen BP.

To investigate the observational signatures of such stochastic GW, our estimated model-dependent GW intensities are compared with the future space-based and ground-based detectors such as ALIA, BBO, DECIGO, aLIGO, aLIGO+ and pulsar timing arrays such as NANOGrav11 and NANOGrav12.5. We are typically interested in the GW spectra from FOPT in a fast expanding universe which lie within the NANOGrav sensitivity. For calculating the thermal parameters related to the phase transition we use the publicly available *CosmoTransition* package [34] and compute the total GW intensities using Eqs. (32)-(46). We choose a benchmark point (BP) with  $m_\phi = 70$  GeV which is safe from Higgs invisible decay constraint. Note that all the scalar couplings giving rise to strong first order PT are  $\lambda_i \sim 0.1$ . As we have checked, a larger scalar mass does not alter our results.

The thermal parameters  $\{v_c, T_c, v_n, T_n, \alpha\}$  for the chosen BP are tabulated in Tab. III. The strength of the FOPT depends on the order parameter  $v_c/T_c$  and the transition is said to be strong enough if it satisfies the condition  $v_c/T_c \geq 1$ , which in our case turns out to be

$v_c/T_c = 1.04$ . In Tab. IV we present the results for GW intensity and corresponding peak frequency for different values of  $n$  and  $T_R$ . From Tab. IV and Fig. 4 we observe that the GW intensity increases and peak shifts to the lower frequency region for smaller values of  $T_R$  at a fixed  $n$ . The GW intensities as a function of frequency are plotted in Fig. 4 for different choices of  $n$  and  $T_R$ . We compare our model-dependent GW intensities with the sensitivity plots of PTAs such as NANOGrav11, NANOGrav12.5 and future space-based, ground-based gravitational wave detectors such as ALIA, BBO, DECIGO, LISA, aLIGO and aLIGO+<sup>1</sup>. From the Fig. 4 one observes that for  $n = 3$ ,  $T_R = 40$  MeV and  $n = 4$ ,  $T_R = 200$  MeV the GW intensity lies within the sensitivity curves of NANOGrav-12.5. There are other choices of  $\{n, T_R\}$  that also give rise to detectable GW intensities which fall within the reach of detectors like ALIA, BBO, DECIGO, LISA and NANOGrav11.

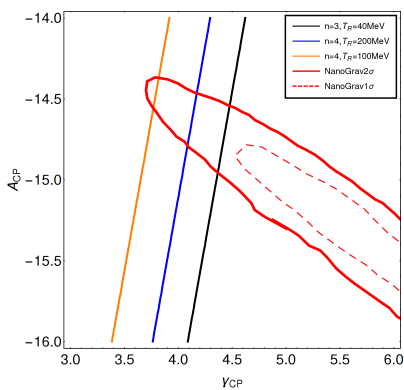


Figure 5. The blue and black solid lines correspond to the predictions of  $\gamma_{\text{CP}}$  and  $A_{\text{CP}}$  (with  $A_{\text{CP}}$  the characteristic GW strain amplitude at  $f = \text{yr}^{-1}$  and  $\gamma_{\text{CP}}$  the spectral index of the pulsar timing-residual cross-power spectral density) obtained for different fixed values of  $\{n, T_R\}$  which gives rise to  $\Omega_{\text{GW}} h^2$  required to explain the NANOGrav result. The dashed and solid red curves correspond to the  $1\sigma$  and  $2\sigma$   $\gamma_{\text{CP}}-A_{\text{CP}}$  contours obtained by NANOGrav 12.5 yrs dataset.

The results of PTA GW searches are generally reported in terms of a pulsar timing-residual cross-power spectral density which has a frequency dependence of the form  $f^{-\gamma_{\text{CP}}}$ . Corresponding power spectrum of the characteristic GW strain is usually approximated as a power-law of the form

$$h_c(f) = A_{\text{CP}} \left( \frac{f}{f_{\text{yr}}} \right)^{\alpha_{\text{CP}}} \quad (48)$$

with  $\alpha_{\text{CP}} = (3 - \gamma_{\text{CP}})/2$  which is  $-2/3$  for a population of inspiraling supermassive black holes (SMBHB)

in circular orbits whose evolution is dominated by GW emission. Most importantly, The reference frequency is given by  $f = \text{yr}^{-1}$ . The power spectrum is related to the GW energy density via [66]

$$\Omega_{\text{GW}} = \frac{2\pi^2}{3\mathcal{H}^2} f^2 h_c^2(f). \quad (49)$$

$n$	$T_R$ in MeV	$\frac{\beta}{\mathcal{H}}$	$f_{\text{peak}}$ in Hz	$\Omega_{\text{GW}} h_{\text{peak}}^2$
-	-	5264.70	$3.45 \times 10^{-2}$	$1.95 \times 10^{-19}$
1	16	57.53	$3.76 \times 10^{-4}$	$2.72 \times 10^{-14}$
2	10	0.39	$2.57 \times 10^{-6}$	$3.49 \times 10^{-11}$
3	40	0.027	$1.78 \times 10^{-7}$	$7.30 \times 10^{-9}$
4	200	0.012	$7.68 \times 10^{-8}$	$3.91 \times 10^{-8}$
4	100	0.0029	$1.92 \times 10^{-8}$	$6.26 \times 10^{-7}$

Table IV. The calculated values of peak frequencies and corresponding GW intensity for the standard cosmology scenario (first row) and non-standard scenarios with different choices of  $T_R$ .

The GW search results due to PTA are reported in terms of joint  $A_{\text{CP}} - \gamma_{\text{CP}}$  posterior distributions or as the posterior distribution at a fiducial value of  $\gamma_{\text{CP}}$  [1, 66]. NANOGrav collaboration has obtained joint constraints on  $A_{\text{CP}}$  and  $\gamma_{\text{CP}}$  by fitting the power-law in Eq. (48) [1]. Since Eq. (49) is a function of  $n, T_R$  (through  $\mathcal{H}$ ), hence it is possible to project limits on the fast expansion parameters by exploiting Eq. (48). Now, as we have shown in Fig. 4, corresponding to  $n = 3, 4$  the GW intensities overlap with the NANOGrav sensitivity curves. We thus cast  $n - T_R$  constraints from Fig. 4 onto the  $A_{\text{CP}} - \gamma_{\text{CP}}$  plane with corresponding  $1\sigma$  and  $2\sigma$  contours from NANOGrav result [1]. Here we observe that for a fixed  $n = 4$  a larger  $T_R$  shifts the straight line contour (orange) to the edge of the  $2\sigma$  contour (red thick), while smaller  $n$  (black) is closer to the  $1\sigma$  contour (red dashed). From Fig. 4 and 5 we see that NANOGrav results not only support a faster expansion in the pre-BBN era, also favour  $n \lesssim 4$  for certain choices of  $T_R$ . Based on the analysis in Sec. III and Sec. IV we can infer that while right relic abundance for the DM can be obtained for any  $n > 0$  by properly tuning the cut-off scale, reheat temperature and  $T_R$  but explaining NANOGrav results from a SFOPt together with the right DM abundance necessarily demands  $n \lesssim 4$  and  $T_R \lesssim \mathcal{O}(100)$  MeV.

## V. POSSIBLE UV COMPLETION

Here we would like to elucidate a possible UV complete framework of the effective Lagrangian we discussed in Eq. (14). There might be several possibilities to obtain an effective interaction of the form in Eq. (14). For an instance, the authors in [67] have discussed one such alternative. However, in their case the  $Z_4$  is broken by

<sup>1</sup>In this work we use the power-law-integrated sensitivity curves following [57, 62]. One can also use the other methods to represent the sensitivity curves [63–65]

the non-zero VEV of the singlet scalar  $\phi$  leading to a remnant  $Z_2$  symmetry under which the extra fermions are odd (DM). On the other hand, in [68] a  $Z_2$  symmetry has been imposed under which all the fields in the dark sector are odd. Here we would like to furnish the simplest possible model remembering the fact that in the present scenario the singlet scalar does not acquire any tree-level VEV. This is in contrast to the set-up discussed in [69] where the singlet fermionic WIMP-like DM is stabilized by a  $Z_2$  symmetry and the singlet scalar acquires a VEV providing a strongly first order electroweak phase transition.

Fields	$SU(2)_L$	$U(1)_Y$	$Z_4$
$\chi$	1	0	$i$
$\psi^T : (\psi^0, \psi^-)$	1	1/2	$-i$
$\phi$	1	0	$-1$

Table V. Charges of different fields appearing in a possible UV completion of the Lagrangian in Eq. (14).

We assume a dark sector that is made up of a vector like lepton (VLL) singlet  $\chi$  and a  $SU(2)_L$  VLL doublet  $\psi$  with the charges as mentioned in Tab. V. As mentioned earlier, we consider the new particles transform under a  $Z_4$  symmetry with their charges as in Tab. V. With the given  $SM \times Z_4$  symmetry the renormalizable Lagrangian can be written as

$$\mathcal{L} \supset m_\chi \bar{\chi}\chi + M_\psi \bar{\psi}\psi + Y \bar{\psi} \tilde{H} \chi + y_\chi \bar{\chi} \phi + \text{H.c.} \quad (50)$$

At a scale  $\mu \ll M_\psi$  the heavy VLLs can be integrated out, resulting in operators of the form  $(H^\dagger H) (\bar{\chi}\chi) / M_\psi$ . If the reheat temperature of the universe is smaller than  $M_\psi$  then the additional VLLs are not present in the thermal bath and the resulting DM-SM interaction mimics a dimension five operator with cut-off scale  $\Lambda \equiv M_\psi$ .

## VI. CONCLUSION

In this paper we have studied a simple framework where it is possible to address both dark matter (DM) relic abundance via freeze-in and the recent NANOGrav result from a strong first order phase transition (SFOPT) in a fast expanding universe. In order to accomplish them together, we consider a dark sector consisting of a SM gauge singlet fermion  $\chi$  and a scalar singlet  $\phi$  both charged under a  $Z_4$  symmetry. We consider  $\chi$  to be the lightest stable fermion in the dark sector that can serve as a viable DM candidate. Being singlet under SM gauge symmetry the dark fermion does not have any interactions in the renormalizable level with the SM fields. The scalar, on the other hand, remains in equilibrium with the thermal bath via non-negligible portal coupling and is responsible in generating SFOPT.

We focus on the DM genesis via freeze-in, typically UV freeze-in, as the dark sector and the visible sector are con-

joined through non-renormalizable interaction of dimension five. The DM yield is computed by taking into account all processes leading to DM production both before and after the electroweak symmetry breaking (EWSB). While the processes before EWSB (dominantly UV) are only  $2 \rightarrow 2$  scattering channels producing DM pair in the final state, after EWSB a host of annihilation and decay channels appear which contribute to both UV and IR freeze-in of the DM. From the requirement of obtaining the observed DM abundance we put constraints on the fast expansion parameters  $T_R, n$  for fixed DM masses. This also put constraints on the other two relevant free parameters of the model, namely the effective scale  $\Lambda$  and the reheat temperature  $T_{RH}$  which we consider to  $T_{RH} \gtrsim 1$  TeV. We see, in accordance with previously reported results, in a faster-than-standard expanding universe, freeze-in production is hugely suppressed for any  $n > 0$ . This, in turn, implies that to produce enough DM via freeze-in to match observations, one has to bring down the effective scale of interaction (equivalently, the DM-SM coupling) substantially with respect to the standard cosmological scenario.

The presence of the scalar singlet facilitates strong first order phase transition (SFOPT) which is otherwise impossible to achieve within the SM particle content. In the presence of fast expansion, we observe, such SFOPT gives rise to gravitational wave (GW) signal with intensities that are detectable by several space-based and ground-based GW detectors. In a fast expanding universe such strong GW signals can be generated for  $\lambda_{H\phi} \gtrsim 0.1$  unlike the standard cosmological scenario which requires large enough portal coupling. The GW signal thus generated can explain the 12.5-year pulsar timing data due to NANOGrav. However, SFOPT supporting NANOGrav result is possible only for specific choices of the parameters that control the fast expansion. Typically, we see  $n \lesssim 4$  lies within the  $2\sigma$  posterior contours for amplitude and spectral slope obtained by the NANOGrav collaboration. For all such  $n \lesssim 4$  the cut-off scale turns out to be  $\Lambda \gtrsim 10^{10}$  GeV that can well explain observed DM abundance for suitable choice of the temperature  $T_R \sim \mathcal{O}(100)$  MeV. Thus, a simple framework of the kind discussed here connects reheat temperature of the universe with a SFOPT in a fast expanding cosmological background. A possible underlying UV complete theory which can give rise to such dimension-5 effective interactions have also been discussed briefly. It will however be interesting, in the context of a UV complete theory, to look into interplay of different parameters giving rise to DM relic abundance and a stochastic GW signal in a fast expanding universe, together with more exotic physics. We shall address such issues in forthcoming works.

## ACKNOWLEDGEMENTS

BB would like to acknowledge discussions with Abhijit Kumar Saha, Debasish Borah and e-mail conversa-

tions Sunny Vagnozzi. AP would like to thank Biswajit Banerjee for the implementation of the CosmoTransition

package. Work of ADB is supported in part by the National Science Foundation of China (11775093, 11422545, 11947235).

- 
- [1] Z. Arzoumanian *et al.* (NANOGrav), (2020), [arXiv:2009.04496 \[astro-ph.HE\]](#).
- [2] A. Sesana, F. Haardt, P. Madau, and M. Volonteri, *Astrophys. J.* **611**, 623 (2004), [arXiv:astro-ph/0401543](#).
- [3] J. Ellis and M. Lewicki, (2020), [arXiv:2009.06555 \[astro-ph.CO\]](#).
- [4] S. Blasi, V. Brdar, and K. Schmitz, (2020), [arXiv:2009.06607 \[astro-ph.CO\]](#).
- [5] S. Chigusa, Y. Nakai, and J. Zheng, (2020), [arXiv:2011.04090 \[hep-ph\]](#).
- [6] A. Neronov, A. Roper Pol, C. Caprini, and D. Semikoz, (2020), [arXiv:2009.14174 \[astro-ph.CO\]](#).
- [7] Y. Nakai, M. Suzuki, F. Takahashi, and M. Yamada, (2020), [arXiv:2009.09754 \[astro-ph.CO\]](#).
- [8] A. Addazi, Y.-F. Cai, Q. Gan, A. Marciano, and K. Zeng, (2020), [arXiv:2009.10327 \[hep-ph\]](#).
- [9] S. Bhattacharya, S. Mohanty, and P. Parashari, (2020), [arXiv:2010.05071 \[astro-ph.CO\]](#).
- [10] E. W. Kolb and M. S. Turner, *Front. Phys.* **69**, 1 (1990).
- [11] F. D’Eramo, N. Fernandez, and S. Profumo, *JCAP* **05**, 012 (2017), [arXiv:1703.04793 \[hep-ph\]](#).
- [12] F. D’Eramo, N. Fernandez, and S. Profumo, *JCAP* **02**, 046 (2018), [arXiv:1712.07453 \[hep-ph\]](#).
- [13] F. Elahi, C. Kolda, and J. Unwin, *JHEP* **03**, 048 (2015), [arXiv:1410.6157 \[hep-ph\]](#).
- [14] S.-L. Chen and Z. Kang, *JCAP* **05**, 036 (2018), [arXiv:1711.02556 \[hep-ph\]](#).
- [15] N. Bernal, F. Elahi, C. Maldonado, and J. Unwin, *JCAP* **1911**, 026 (2019), [arXiv:1909.07992 \[hep-ph\]](#).
- [16] P. A. R. Ade *et al.* (Planck), *Astron. Astrophys.* **571**, A16 (2014), [arXiv:1303.5076 \[astro-ph.CO\]](#).
- [17] N. Aghanim *et al.* (Planck), (2018), [arXiv:1807.06209 \[astro-ph.CO\]](#).
- [18] N. Bernal and F. Hajkarim, *Phys. Rev. D* **100**, 063502 (2019), [arXiv:1905.10410 \[astro-ph.CO\]](#).
- [19] S. Bhattacharya, S. Mohanty, and P. Parashari, *Phys. Rev. D* **102**, 043522 (2020), [arXiv:1912.01653 \[astro-ph.CO\]](#).
- [20] N. Bernal, A. Ghoshal, F. Hajkarim, and G. Lambiase, (2020), [arXiv:2008.04959 \[gr-qc\]](#).
- [21] B. Ratra and P. J. E. Peebles, *Phys. Rev. D* **37**, 3406 (1988).
- [22] L. J. Hall, K. Jedamzik, J. March-Russell, and S. M. West, *JHEP* **03**, 080 (2010), [arXiv:0911.1120 \[hep-ph\]](#).
- [23] N. Bernal, M. Heikinheimo, T. Tenkanen, K. Tuominen, and V. Vaskonen, *Int. J. Mod. Phys. A* **32**, 1730023 (2017), [arXiv:1706.07442 \[hep-ph\]](#).
- [24] J. Edsjo and P. Gondolo, *Phys. Rev. D* **56**, 1879 (1997), [arXiv:hep-ph/9704361](#).
- [25] B. Barman, S. Bhattacharya, and B. Grzadkowski, (2020), [arXiv:2009.07438 \[hep-ph\]](#).
- [26] A. De Simone, V. Sanz, and H. P. Sato, *Phys. Rev. Lett.* **105**, 121802 (2010), [arXiv:1004.1567 \[hep-ph\]](#).
- [27] D. J. Chung, E. W. Kolb, and A. Riotto, *Phys. Rev. D* **60**, 063504 (1999), [arXiv:hep-ph/9809453](#).
- [28] T. Moroi, H. Murayama, and M. Yamaguchi, *Phys. Lett. B* **303**, 289 (1993).
- [29] M. Kawasaki and T. Moroi, *Prog. Theor. Phys.* **93**, 879 (1995), [arXiv:hep-ph/9403364](#).
- [30] L. Kofman, A. D. Linde, and A. A. Starobinsky, *Phys. Rev. D* **56**, 3258 (1997), [arXiv:hep-ph/9704452](#).
- [31] A. D. Linde, *Particle physics and inflationary cosmology*, Vol. 5 (1990) [arXiv:hep-th/0503203](#).
- [32] B. Barman, D. Borah, and R. Roshan, *JCAP* **11**, 021 (2020), [arXiv:2007.08768 \[hep-ph\]](#).
- [33] M. Kakizaki, S. Kanemura, and T. Matsui, *Phys. Rev. D* **92**, 115007 (2015), [arXiv:1509.08394 \[hep-ph\]](#).
- [34] C. L. Wainwright, *Comput. Phys. Commun.* **183**, 2006 (2012), [arXiv:1109.4189 \[hep-ph\]](#).
- [35] S. R. Coleman and E. J. Weinberg, *Phys. Rev.* **D7**, 1888 (1973).
- [36] P. Basler, M. Krause, M. Muhlleitner, J. Wittbrodt, and A. Wlotzka, *JHEP* **02**, 121 (2017), [arXiv:1612.04086 \[hep-ph\]](#).
- [37] P. B. Arnold and O. Espinosa, *Phys. Rev.* **D47**, 3546 (1993), [Erratum: *Phys. Rev.*D50,6662(1994)], [arXiv:hep-ph/9212235 \[hep-ph\]](#).
- [38] A. Kosowsky, M. S. Turner, and R. Watkins, *Phys. Rev.* **D45**, 4514 (1992).
- [39] A. Paul, B. Banerjee, and D. Majumdar, *JCAP* **1910**, 062 (2019), [arXiv:1908.00829 \[hep-ph\]](#).
- [40] A. Kosowsky and M. S. Turner, *Phys. Rev.* **D47**, 4372 (1993), [arXiv:astro-ph/9211004 \[astro-ph\]](#).
- [41] S. J. Huber and T. Konstandin, *JCAP* **0809**, 022 (2008), [arXiv:0806.1828 \[hep-ph\]](#).
- [42] A. Kosowsky, M. S. Turner, and R. Watkins, *Phys. Rev. Lett.* **69**, 2026 (1992).
- [43] M. Kamionkowski, A. Kosowsky, and M. S. Turner, *Phys. Rev.* **D49**, 2837 (1994), [arXiv:astro-ph/9310044 \[astro-ph\]](#).
- [44] C. Caprini, R. Durrer, and G. Servant, *Phys. Rev.* **D77**, 124015 (2008), [arXiv:0711.2593 \[astro-ph\]](#).
- [45] M. Hindmarsh, S. J. Huber, K. Rummukainen, and D. J. Weir, *Phys. Rev. Lett.* **112**, 041301 (2014), [arXiv:1304.2433 \[hep-ph\]](#).
- [46] J. T. Giblin, Jr. and J. B. Mertens, *JHEP* **12**, 042 (2013), [arXiv:1310.2948 \[hep-th\]](#).
- [47] J. T. Giblin and J. B. Mertens, *Phys. Rev.* **D90**, 023532 (2014), [arXiv:1405.4005 \[astro-ph.CO\]](#).
- [48] M. Hindmarsh, S. J. Huber, K. Rummukainen, and D. J. Weir, *Phys. Rev.* **D92**, 123009 (2015), [arXiv:1504.03291 \[astro-ph.CO\]](#).
- [49] C. Caprini and R. Durrer, *Phys. Rev.* **D74**, 063521 (2006), [arXiv:astro-ph/0603476 \[astro-ph\]](#).
- [50] T. Kahniashvili, A. Kosowsky, G. Gogoberidze, and Y. Maravin, *Phys. Rev.* **D78**, 043003 (2008), [arXiv:0806.0293 \[astro-ph\]](#).
- [51] T. Kahniashvili, L. Campanelli, G. Gogoberidze, Y. Maravin, and B. Ratra, *Phys. Rev.* **D78**, 123006 (2008), [Erratum: *Phys. Rev.*D79,109901(2009)], [arXiv:0809.1899 \[astro-ph\]](#).

- [52] T. Kahniashvili, L. Kisslinger, and T. Stevens, *Phys. Rev.* **D81**, 023004 (2010), [arXiv:0905.0643 \[astro-ph.CO\]](#).
- [53] C. Caprini, R. Durrer, and G. Servant, *JCAP* **0912**, 024 (2009), [arXiv:0909.0622 \[astro-ph.CO\]](#).
- [54] B. Barman, A. Dutta Banik, and A. Paul, *Phys. Rev. D* **101**, 055028 (2020), [arXiv:1912.12899 \[hep-ph\]](#).
- [55] A. Paul, U. Mukhopadhyay, and D. Majumdar, (2020), [arXiv:2010.03439 \[hep-ph\]](#).
- [56] P. J. Steinhardt, *Phys. Rev.* **D25**, 2074 (1982).
- [57] P. S. B. Dev, F. Ferrer, Y. Zhang, and Y. Zhang, *JCAP* **1911**, 006 (2019), [arXiv:1905.00891 \[hep-ph\]](#).
- [58] V. R. Shajiee and A. Tofighi, *Eur. Phys. J.* **C79**, 360 (2019), [arXiv:1811.09807 \[hep-ph\]](#).
- [59] C. Caprini et al., *JCAP* **1604**, 001 (2016), [arXiv:1512.06239 \[astro-ph.CO\]](#).
- [60] J. Ellis, M. Lewicki, and J. M. No, (2018), [10.1088/1475-7516/2019/04/003](#), [JCAP1904,003(2019)], [arXiv:1809.08242 \[hep-ph\]](#).
- [61] J. Ellis, M. Lewicki, J. M. No, and V. Vaskonen, *JCAP* **1906**, 024 (2019), [arXiv:1903.09642 \[hep-ph\]](#).
- [62] E. Thrane and J. D. Romano, *Phys. Rev.* **D88**, 124032 (2013), [arXiv:1310.5300 \[astro-ph.IM\]](#).
- [63] K. Schmitz, (2020), [arXiv:2002.04615 \[hep-ph\]](#).
- [64] C. Moore, R. Cole, and C. Berry, *Class. Quant. Grav.* **32**, 015014 (2015), [arXiv:1408.0740 \[gr-qc\]](#).
- [65] T. Alanne, T. Hugle, M. Platscher, and K. Schmitz, *JHEP* **03**, 004 (2020), [arXiv:1909.11356 \[hep-ph\]](#).
- [66] S. Vagnozzi, (2020), [arXiv:2009.13432 \[astro-ph.CO\]](#).
- [67] A. Dutta Banik, A. K. Saha, and A. Sil, *Phys. Rev. D* **98**, 075013 (2018), [arXiv:1806.08080 \[hep-ph\]](#).
- [68] P. Konar, A. Mukherjee, A. K. Saha, and S. Show, (2020), [arXiv:2007.15608 \[hep-ph\]](#).
- [69] M. Fairbairn and R. Hogan, *JHEP* **09**, 022 (2013), [arXiv:1305.3452 \[hep-ph\]](#).